Supplement of Atmos. Chem. Phys., 15, 3687–3701, 2015
http://www.atmos-chem-phys.net/15/3687/2015/
doi:10.5194/acp-15-3687-2015-supplement

Atmospheric Chemistry and Physics Open Access

Supplement of

Submicron particle mass concentrations and sources in the Amazonian wet season (AMAZE-08)

Q. Chen et al.

Correspondence to: S. T. Martin (scot_martin@harvard.edu) and P. Artaxo (artaxo@if.usp.br)

A. AMS sampling and data processing

Chen et al. (2009) described the AMS sampling and data processing. Additional details are provided herein. Standard relative ionization efficiencies (RIE) were used in the analysis, including 1.1 for nitrate, 1.2 for sulfate, 1.4 for organic molecules, 4.0 for ammonium, 1.3 for chloride, and 2.0 for water (DeCarlo et al., 2006; Mensah et al., 2011). Unlike the analysis in Chen et al. (2009), the organic signals of C_3H^+ at *m*/*z* 37, $C_3H_2^+$ at *m*/*z* 38, $C_3H_3^+$ at *m*/*z* 39, and $C_3H_4^+$ at *m*/*z* 40, which made up 5-8% of the total organic signal, were calculated time-dependently based on the ratio of them to $C_2H_2^+$ at *m*/*z* 26. In the present study particle-phase water was not included in the calculations of species mass concentrations. Occasionally the sampling site was influenced by the exhaust plumes from the site power source, which was a diesel generator located 0.72 km from TT34 and typically downwind. Abrupt increases in AMS-measured sulfate mass concentrations, even greater than the organic concentrations, were indicators of influence by the local pollution source. These pollution events were defined herein and excluded from the data sets analyzed (Fig. 1). Chen et al. (2009) excluded more data by using a broader pollution filter defined by Martin et al. (2010).

The AMS detection limits, calculated as three times the standard deviation of mass concentrations for filtered air obtained at 150-s intervals, were 0.06, 0.02, 0.001, 0.006, 0.002 $\mu g\ m^{-3}$ for organic material, sulfate, ammonium, chloride, and nitrate, respectively. The AMS is capable of focusing particles with 30-1000 nm with size-dependent particle transmission efficiency (Liu et al., 2007). As described in Gunthe et al. (2009), we operated the AMS at

sampling pressures of 867–907 hPa. Under these conditions, the transmission efficiency is close to 100% for particles with vacuum aerodynamic diameter d_{va} of 100–400 nm and is greater than 20% for particles with d_{va} of 50-1000 nm. For organic measurements, the estimated uncertainty is 30% at concentrations of 1 μg m^{-3} to 40% at concentrations of 0.5 μg m^{-3}. It can increase to 100% for low organic concentrations (0.1 μg m^{-3}). For sulfate measurements, the uncertainty is <10% for high concentrations (0.5 μg m^{-3}) and about 40% for low concentrations (0.05 μg m^{-3}).

Atomic ratios of oxygen-to-carbon (O:C), hydrogen-to-carbon (H:C), and nitrogen-to-carbon (N:C), as well as the mass ratios of organic material to organic carbon (OM:OC), were calculated from the W-mode data following previously described methods (Aiken et al., 2008). A recent study shows that organic aerosol with mixed keto-, hydroxyl-, and acid-functionalities readily undergoes thermally-induced dehydration and decarboxylation on the AMS vaporizer (Canagaratna et al., 2015). Such dehydration and decarboxylation can lead to much greater $(CO^+)_{org}$:$(CO_2^+)_{org}$ and $(H_2O^+)_{org}$:$(CO_2^+)_{org}$ ratios than the ones that have been empirically used in the "general" elemental analysis described by Aiken et al. (2008). A correction of 34% increase in O:C and 17% increase in H:C was applied based on the correction formula reported by Canagaratna et al. (2015).

In the AMS, the organosulfate species can fragment to organic ions ($C_xH_yO_z^+$), organosulfur ions ($C_xH_yO_zS^+$), and ions with a pattern indistinguishable from inorganic sulfate (e.g., SO_2^+) (Farmer et al., 2010). Similarly, the organonitrate species also fragment to the NO_x^+ ions and are detected as inorganic nitrate by the AMS. For the AMAZE-08 data set, signal intensities for $C_xH_yO_zS^+$ ions were not above noise in the collected high-resolution mass spectra. The agreement among AMS, ion chromatography (IC), and particle-induced X-ray emission (PIXE) sulfate mass concentrations, as well as the absence of organosulfur ions in the

high-resolution mass spectra, suggest minimal mass concentration of organosulfate species, at least at concentrations above uncertainty levels. Nitrate had a campaign-average concentration of 7 ± 2 ng m^{-3}. This value was greater than the average fine-mode concentration of 4 ± 1 ng m^{-3} measured by IC. As a test against possible significance of organonitrate species to the results of the present study, a limiting assumption that assigns all AMS-measured nitrate to organonitrate increases the average O:C ratio by <0.01 for the elemental analysis and corresponds to a maximum of 5% contribution of organonitrates to the total organic particle mass concentration for an assumed molecular weight of 360 g mol^{-1} (Chen et al., 2011). The low mass concentration of particle-phase organonitrates is expected because of the low prevailing NO_x concentrations and humid environment (Day et al., 2010; Liu et al., 2012).

B. Other concurrent measurements and comparisons among measurements

Instruments making measurements during AMAZE-08 at the TT34 site are listed in Martin et al. (2010). The size distribution of particles between 0.010 and 0.48 μm (mobility diameter) was measured every 5 min by a Scanning Mobility Particle Sizer (Lund SMPS) (Roldin, 2008). Particle volume concentrations were calculated from the SMPS size distributions for an assumption of spherical particles. The total number concentration for particles greater than 0.010 μm was measured every 3 s by a Condensation Particle Counter (CPC, TSI 3010). Particle scattering coefficients at multiple wavelengths were measured every 1 min by a nephelometer (TSI 3563) and averaged to 10 min. The light absorption at 637 nm of deposited particles was measured every 1 min by the Multiangle Absorption Photometer (MAAP, Thermo 5012). These several instruments sampled through a laminar-flow line (i.e., separate sampling from the AMS line) that was characterized by lower and upper limits of transmission for particle diameters of 0.004 and 7 μm, respectively (Martin et al., 2010). Several particle filter samples were collected

(Artaxo et al., 2013). Total-particle filters (TPF; PM_3) were collected in-line with the turbulent inlet used by the AMS. Stacked filter units (SFU) were installed separately at 10 m to sample fine- (PM_2) and coarse-mode particles (PM_{2-10}). The two types of filters show reasonable agreement on the particle mass concentration (Table S2). The fine-mode data from the SFU are reported herein. Filter samples were analyzed by IC for water-soluble ionic components, including sulfate, nitrate, and ammonium, among other components. The filters were also analyzed by PIXE for elemental composition. Concentrations were adjusted to STP conditions.

The AMS data can be compared to other concurrent measurements of AMAZE-08. The mass ratio of NR-PM_1 measured by the AMS to PM_2 by filter assays was 0.65 as a campaign average (Table S2). The ratio was less than unity because PM_2 included contributions by black carbon and mineral dust (Sect. 3.1) as well as organic material in the diameter range of 1 to 2 μm (Pöschl et al., 2010). Particle mass-diameter distributions obtained from gravimetric analysis of stages of a Multi-Orifice Uniform Deposit Impactor (MOUDI) showed that an average of 30% of the particle mass concentration was associated with diameter range from 1 to 2 μm (cf. Fig. 16 in Martin et al. (2010)).

Figure S6a shows a line of slope m of 1.24 and correlation R^2 of 0.81 in a scatter plot between the AMS-calculated and the SMPS-derived particle volume concentrations. Figure S6b shows the scatter plot of the number concentrations obtained by integrating the SMPS measurements and those directly measured by the CPC. The slope of 0.6 (R^2 = 0.90) indicates that the CPC measured more particles than the corresponding SMPS-derived quantity. The SMPS bias to particle undercounting can explain $m > 1$ in the scatter plot of Fig. S6a. The scatter plot between sulfate particle mass concentrations measured by the AMS and those measured by IC analysis of the filters is fit by a line of m = 0.90 and R^2 = 0.50 (Fig. S6c).

The combined AMS and SMPS data sets were used to estimate the particle effective density ρ_{eff} (kg m^{-3}) based on an in-common mode diameter (Katrib et al., 2005). For nonporous spherical particles, material density ρ has the same values as ρ_{eff}, and this condition was assumed to hold in the performed data analysis. The organic material density ρ_{org} was then derived by assuming volume additivity and by using ρ_{inorg} of 1780 kg m^{-3} for ammonium bisulfate and ρ_{inorg} of 1770 kg m^{-3} for other inorganic components (Cross et al., 2007). The estimated campaign-average value of ρ_{eff} for submicron Amazonian particles is 1390 ± 150 kg m^{-3}. Figure S7 shows one example of the mass-diameter distribution measured by the AMS compared to that derived from the SMPS measurements. Assuming that the chemical components either do not mix or alternatively have a numerically small excess volume of mixing, we can derive ρ_{org} of 1270 ± 110 kg m^{-3} based on the campaign-average chemical composition. The value of ρ_{org} is consistent with the density of 1200-1500 kg m^{-3} observed for laboratory-generated biogenic secondary organic material (Bahreini et al., 2005; Chen et al., 2012; Shilling et al., 2009) and the predicted value of 1310 kg m^{-3} based on the corrected elemental ratios (Kuwata et al., 2012).

Figure S6d shows the linear regression of the light scattering derived from the AMS (PM_1) and the nephelometer measurements (PM_7), all for 550-nm wavelength. In total, 74 time periods having nearly identical mass concentrations of sulfate were selected to obtain the averaged particle mass-diameter distributions measured by the AMS. For comparison, nephelometer data at 550 nm were averaged for the same time periods. The mass-diameter distributions were multiplied by diameter-dependent mass extinction efficiencies (m^2 g^{-1}) to estimate light scattering coefficients. The mass extinction efficiencies were calculated at 550 nm using Mie theory for a refractive index of $1.42 - 0.006i$ (Guyon et al., 2003). An agreement was found between calculated and measured aerosol scattering coefficients, particularly for periods free of

influence of long-range advection of mineral dust. During the period of 22 February to 3 March 2008, the ratio of the AMS volume concentration to the nephelometer scattering is high (Fig. S8b). Elevated mass concentrations of mineral dust are observed by the lidar measurements (Baars et al., 2011) and the filter-based PIXE analysis (Prenni et al., 2009). Local wind and Hysplit back trajectories showed a Manaus plume on March 1, 2008. The elevated scattering is, therefore, plausibly a combination of African advection and Manaus plume influence although the coarse-mode contribution from mineral dust is the major driving force of the a weak correlation (R^2 = 0.21) between the nephelometer and AMS dataset. In contrast, a strong correlation (m = 0.62; R^2 = 0.82) of the two data sets is shown for other periods, suggesting a dominant contribution of the non-refractory submicron volume to the total particle scattering. This non-refractory submicron volume is mainly organic material. The scattering coefficients related to the submicron organic material can go up to 6 Mm^{-1} at 550 nm.

C. Positive-Matrix Factorization

Positive-matrix factorization (PMF) is a receptor-based model using a weighted least squares method to identify patterns in data. With caveats, it can be a useful tool to derive the source profiles of organic components from AMS data sets (Ulbrich et al., 2009). In this study, the PMF analysis was conducted on the V-mode organic UMR spectra (m/z 12 to 220). The spectra were analyzed using the SQUIRREL tookit. Prior to PMF analysis, the data set was pre-filtered to remove inorganic contributions, and the analysis was carried out only on the residual data set of the organic component. Fifteen m/z values were omitted because of the absence of organic ions. The time periods associated with random spikes, abrupt increase in sulfate mass concentrations, and little temporal variation caused by the instrument adjustments (Fig. 1) were removed. The error values were calculated using the method described by Ulbrich et al. (2009).

Fragments having a signal-to-noise ratio less than 2 and fragments set proportionally to *m*/*z* 44 were downweighted by increasing their error estimates (Ulbrich et al., 2009). C_xF_y ions contributed significantly to the signals at *m*/*z* 69, 119, 131, 169, 181, and 219, indicating the contamination of Fomblin lubricating oil, possibly from instrument pumps at the site (Cross et al., 2009). These signals appeared always as one statistical factor, with a spiky time series for the loading of that factor. These fragments were downgraded by increasing their error by 100 times. The PMF analysis was conducted with (1) different model error and (2) different seed number. The former was introduced to add modeling uncertainty to the instrumental uncertainty, reflecting the errors that may occur when the true factors do not have constant mass spectra. The latter represents the pseudo-random starting values. Unless otherwise noted, results are presented for both the model error and the seed number of zero. PMF produces a fit to the data, which is called a solution. The solution contains a set of factors and concentrations. For AMAZE-08, four statistical factors were identified and labeled as HOA, OOA-1, OOA-2, and OOA-3 (Fig. 4). The four factors HOA, OOA-1, OOA-2, and OOA-3 respectively accounted for 2%, 18%, 14%, and 66% of the variance in the data matrix, implying a residual variance of <1%.

Number p of factors

Several mathematical metrics were used to set the number *p* of factors. The ratio Q:Q_{exp} of the sum of the squares of the uncertainty-weighted residuals to the expected values decreased by 16%, 8%, 3%, and 3% for *p* increasing from 2 to 5. Three or more factors therefore significantly account for the variance of data. The residual was 1% for $p = 2$ or 3 and < 0.3% for $p = 4$. Structure in the residual was significantly reduced by increasing from *p* of 3 to 4 (Fig. S9). For these reasons, a choice of $p = 4$ was made for the PMF analysis.

The choice of $p = 4$ was also evaluated with respect to factor similarity and correlations

of the time series of the factors. Increasing the *p* from 4 to 5 resulted in strong correlation (R^2 = 0.96) among the factors (Fig. S10). No sufficient information from the correlations with other tracers exists to anticipate this correlation; correlation among factors for *p* of 5 is believed to arise from a splitting of real factors.

Rotational ambiguity of solutions (*FPEAK*).

FPEAK is the rotational parameter. For simplicity, *FPEAK* = 0 was used as the best representation of the PMF solution for this study. The PMF solution was evaluated for uniqueness under linear transformations ("rotations") by varying the *FPEAK* parameter (Ulbrich et al., 2009). Solutions with *FPEAK* between -0.6 and 0.6 increase Q:Q_{exp} by 1%. Figure S11 shows the time series of factor concentrations over this *FPEAK* range. Changes in time series are relatively small compared to the changes in the features of the factors. The largest change is for the HOA factor. This factor accounts for a low fraction of the total signal and hence its features can change without causing a great increase in the residual. The rotational uncertainty causes no conflicts in the interpretation of the PMF factors.

Uncertainty of the solutions.

The results of running the PMF analysis for different pseudo-random starting values (i.e., seeds of 0 to 10) show negligible changes in the factors (R^2 > 0.999; m > 0.995) and the time series of the concentrations (R^2 > 0.999; m > 0.95). Testing a "model error" of 5% in the PMF analysis leads to changes in the factor profiles (R^2 > 0.80; m > 0.90) and in the time series of concentrations (R^2 > 0.95; m > 0.75) that are close to tolerance.

Quantitative assessment of the uncertainty of the factors is also made by 100 bootstrapping runs (Ulbrich et al., 2009). The results show that the uncertainties in the time series of the concentrations are 15% for the OOA-2 and OOA-3 factors and 30% for the OOA-1

and HOA factors. The uncertainties in the factor spectra are <4% for OOA-2 and OOA-3 and <9% for OOA-1 and HOA. The mass spectrum of the HOA factor has the largest uncertainty (Fig. S12).

Literature Cited

Aiken, A. C., Decarlo, P. F., Kroll, J. H., Worsnop, D. R., Huffman, J. A., Docherty, K. S., Ulbrich, I. M., Mohr, C., Kimmel, J. R., Sueper, D., Sun, Y., Zhang, Q., Trimborn, A., Northway, M., Ziemann, P. J., Canagaratna, M. R., Onasch, T. B., Alfarra, M. R., Prevot, A. S. H., Dommen, J., Duplissy, J., Metzger, A., Baltensperger, U., and Jimenez, J. L.: O/C and OM/OC ratios of primary, secondary, and ambient organic aerosols with high-resolution time-of-flight aerosol mass spectrometry, Environ. Sci. Technol., 42, 4478-4485, 10.1021/es703009q, 2008.

Artaxo, P., Rizzo, L. V., Brito, J. F., Barbosa, H. M. J., A., A., Sena, E. T., Cirino, G. G., Bastos, W., Martin, S. T., and Andreae, M. O.: Atmospheric aerosols in Amazonia and land use change: from natural biogenic to biomass burning conditions, Faraday Discuss., 165, 1-31, 10.1039/c3fd00052d, 2013.

Baars, H., Ansmann, A., Althausen, D., Engelmann, R., Artaxo, P., Pauliquevis, T., and Souza, R.: Further evidence for significant smoke transport from Africa to Amazonia, Geophys. Res. Lett., 38, L20802, 10.1029/2011GL049200, 2011.

Bahreini, R., Keywood, M. D., Ng, N. L., Varutbangkul, V., Gao, S., Flagan, R. C., Seinfeld, J. H., Worsnop, D. R., and Jimenez, J. L.: Measurements of secondary organic aerosol from oxidation of cycloalkenes, terpenes, and m-xylene using an Aerodyne aerosol mass spectrometer, Environ. Sci. Technol., 39, 5674-5688, 10.1021/es048061a, 2005.

Canagaratna, M. R., Jimenez, J. L., Kroll, J. H., Chen, Q., Kessler, S. H., Massoli, P., Hildebrandt Ruiz, L., Fortner, E., Williams, L. R., Wilson, K. R., Surratt, J. D., Donahue, N. M., Jayne, J. T., and Worsnop, D. R.: Elemental ratio measurements of organic compounds using aerosol mass spectrometry: characterization, improved calibration, and implications, Atmos. Chem. Phys., 15, 253-272, 10.5194/acp-15-253-2015, 2015.

Chen, Q., Farmer, D. K., Schneider, J., Zorn, S. R., Heald, C. L., Karl, T. G., Guenther, A., Allan, J. D., Robinson, N., Coe, H., Kimmel, J. R., Pauliquevis, T., Borrmann, S., Pöschl, U., Andreae, M. O., Artaxo, P., Jimenez, J. L., and Martin, S. T.: Mass spectral characterization of submicron biogenic organic particles in the Amazon Basin, Geophys. Res. Lett., 36, L20806, 10.1029/2009gl039880, 2009.

Chen, Q., Liu, Y., Donahue, N. M., Shilling, J. E., and Martin, S. T.: Particle-phase chemistry of secondary organic material: Modeled compared to measured O:C and H:C elemental ratios provide constraints, Environ. Sci. Technol., 45, 4763-4770, 10.1021/es104398s, 2011.

Chen, Q., Li, Y. L., McKinney, K. A., Kuwata, M., and Martin, S. T.: Particle mass yield from β-caryophyllene ozonolysis, Atmos. Chem. Phys., 12, 3165-3179, 10.5194/acp-12-3165-2012, 2012.

Cross, E. S., Slowik, J. G., Davidovits, P., Allan, J. D., Worsnop, D. R., Jayne, J. T., Lewis, D. K., Canagaratna, M., and Onasch, T. B.: Laboratory and ambient particle density determinations using light scattering in conjunction with aerosol mass spectrometry, Aerosol Sci. Technol., 41, 343-359, 10.1080/02786820701199736, 2007.

Cross, E. S., Onasch, T. B., Canagaratna, M., Jayne, J. T., Kimmel, J., Yu, X. Y., Alexander, M. L., Worsnop, D. R., and Davidovits, P.: Single particle characterization using a light scattering module coupled to a time-of-flight aerosol mass spectrometer, Atmos. Chem. Phys., 9, 7769-7793, 2009.

Day, D. A., Liu, S., Russell, L. M., and Ziemann, P. J.: Organonitrate group concentrations in submicron particles with high nitrate and organic fractions in coastal southern California, Atmos. Environ., 44, 1970-1979, 10.1016/j.atmosenv.2010.02.045, 2010.

DeCarlo, P. F., Kimmel, J. R., Trimborn, A., Northway, M. J., Jayne, J. T., Aiken, A. C., Gonin, M., Fuhrer, K., Horvath, T., Docherty, K. S., Worsnop, D. R., and Jimenez, J. L.: Field-deployable, high-resolution, time-of-flight aerosol mass spectrometer, Anal. Chem., 78, 8281-8289, 10.1021/ac061249n, 2006.

Farmer, D. K., Matsunaga, A., Docherty, K. S., Surratt, J. D., Seinfeld, J. H., Ziemann, P. J., and Jimenez, J. L.: Response of an aerosol mass spectrometer to organonitrates and organosulfates and implications for atmospheric chemistry, Proc. Natl. Acad. Sci. U. S. A., 107, 6670-6675, 10.1073/pnas.0912340107, 2010.

Gunthe, S. S., King, S. M., Rose, D., Chen, Q., Roldin, P., Farmer, D. K., Jimenez, J. L., Artaxo, P., Andreae, M. O., Martin, S. T., and Pöschl, U.: Cloud condensation nuclei in pristine tropical rainforest air of Amazonia: size-resolved measurements and modeling of atmospheric aerosol composition and CCN activity, Atmos. Chem. Phys., 9, 7551-7575, 10.5194/acp-9-7551-2009, 2009.

Guyon, P., Boucher, O., Graham, B., Beck, J., Mayol-Bracero, O. L., Roberts, G. C., Maenhaut, W., Artaxo, P., and Andreae, M. O.: Refractive index of aerosol particles over the Amazon tropical forest during LBA-EUSTACH 1999, J. Aerosol Sci., 34, 883-907, 10.1016/s0021-8502(03)00052-1, 2003.

Katrib, Y., Martin, S. T., Rudich, Y., Davidovits, P., Jayne, J. T., and Worsnop, D. R.: Density changes of aerosol particles as a result of chemical reaction, Atmos. Chem. Phys., 5, 275-291, 2005.

Kuwata, M., Zorn, S. R., and Martin, S. T.: Using elemental ratios to predict the density of organic material composed of carbon, hydrogen, and oxygen, Environ. Sci. Technol., 46, 787-794, 10.1021/es202525q, 2012.

Liu, P. S. K., Deng, R., Smith, K. A., Williams, L. R., Jayne, J. T., Canagaratna, M. R., Moore, K., Onasch, T. B., Worsnop, D. R., and Deshler, T.: Transmission efficiency of an aerodynamic focusing lens system: Comparison of model calculations and laboratory measurements for the Aerodyne Aerosol Mass Spectrometer, Aerosol Sci. Technol., 41, 721-733, 10.1080/02786820701422278, 2007.

Liu, S., Shilling, J. E., Song, C., Hiranuma, N., Zaveri, R. A., and Russell, L. M.: Hydrolysis of organonitrate functional groups in aerosol particles, Aerosol Sci. Technol., 46, 1359-1369, 10.1080/02786826.2012.716175, 2012.

Martin, S. T., Andreae, M. O., Althausen, D., Artaxo, P., Baars, H., Borrmann, S., Chen, Q., Farmer, D. K., Guenther, A., Gunthe, S. S., Jimenez, J. L., Karl, T., Longo, K., Manzi, A., Muller, T., Pauliquevis, T., Petters, M. D., Prenni, A. J., Pöschl, U., Rizzo, L. V., Schneider, J., Smith, J. N., Swietlicki, E., Tota, J., Wang, J., Wiedensohler, A., and Zorn, S. R.: An overview of the Amazonian Aerosol Characterization Experiment 2008 (AMAZE-08), Atmos. Chem. Phys., 10, 11415-11438, 10.5194/acp-10-11415-2010, 2010.

Mensah, A. A., Buchholz, A., Mentel, T. F., Tillmann, R., and Kiendler-Scharr, A.: Aerosol mass spectrometric measurements of stable crystal hydrates of oxalates and inferred relative ionization efficiency of water, J. Aerosol Sci., 42, 11-19, 10.1016/j.jaerosci.2010.10.003, 2011.

Pöschl, U., Martin, S. T., Sinha, B., Chen, Q., Gunthe, S. S., Huffman, J. A., Borrmann, S., Farmer, D. K., Garland, R. M., Helas, G., Jimenez, J. L., King, S. M., Manzi, A., Mikhailov, E., Pauliquevis, T., Petters, M. D., Prenni, A. J., Roldin, P., Rose, D., Schneider, J., Su, H., Zorn, S. R., Artaxo, P., and Andreae, M. O.: Rainforest aerosols as biogenic nuclei of clouds and precipitation in the Amazon, Science, 329, 1513-1516, 10.1126/science.1191056, 2010.

Prenni, A. J., Petters, M. D., Kreidenweis, S. M., Heald, C. L., Martin, S. T., Artaxo, P., Garland, R. M., Wollny, A. G., and Pöschl, U.: Relative roles of biogenic emissions and Saharan dust as ice nuclei in the Amazon basin, Nature Geoscience, 2, 401-404, Doi 10.1038/Ngeo517, 2009.

Roldin, P., Nilsson, E., Swietlicki, E., Massling, A., and Zhou, J.: *Lund SMPS User's manual*, EUCAARI Brazil Version, 2008.

Shilling, J. E., Chen, Q., King, S. M., Rosenoern, T., Kroll, J. H., Worsnop, D. R., DeCarlo, P. F., Aiken, A. C., Sueper, D., Jimenez, J. L., and Martin, S. T.: Loading-dependent elemental composition of α-pinene SOA particles, Atmos. Chem. Phys., 9, 771-782, 10.5194/acp-9-771-2009, 2009.

Ulbrich, I. M., Canagaratna, M. R., Zhang, Q., Worsnop, D. R., and Jimenez, J. L.: Interpretation of organic components from Positive Matrix Factorization of aerosol mass spectrometric data, Atmos. Chem. Phys., 9, 2891-2918, 2009.

Table S1. Summary of the regression coefficients *m* of instrument comparisons. Expected *m* values are shown in parentheses. These values are estimated on the basis of the diameter domain of the various instruments and an assumed AMS collection efficiency of 1.0, in conjunction with typical mass size distributions obtained by MOUDI measurements during the wet season in the Amazon basin (Martin et al., 2010; Pöschl et al., 2010).

	Volume concentration	Number concentration	Sulfate mass concentration	Particle mass concentration	Light scattering at 550 nm
	SMPS	CPC	Filter-based	Filter-based	Nephelometer
AMS	1.24 (1.0)	-	0.90 (1.0)	0.65 (0.7)	0.62 (< 1.0)
SMPS	-	0.59 (< 1.0)	-	-	

Table S2. Summary of the particle mass concentration (μg m^{-3}, STP) measured by the stacked filter units on the 10-m inlet (SFU), by the total-particle filter on the 38-m turbulent inlet (TPF), and by the AMS during AMAZE-08.

Sampling Periods (MM/DD/YY)	SFU: PM_2	TPF: PM_3	AMS: NR-PM_1	AMS/SFU	AMS/TPF
02/10/08 – 02/14/08	2.51	n.a.	1.75	0.70	n.a.
02/14/08 – 02/16/08	1.41	1.30	1.37	0.97	0.87
02/16/08 – 02/19/08	0.87		0.89	1.02	
02/19/08 – 02/22/08	1.14	1.48	0.85	0.75	0.57
02/22/08 – 02/26/08	2.44		0.85	0.35	
02/26/08 – 02/29/08	3.20	2.86	0.96	0.30	0.33
02/29/08 – 03/04/08	3.38		0.99	0.29	
03/04/08 – 03/08/08	1.02	1.02	0.73	0.72	0.72
03/08/08 – 03/12/08	1.01	1.09	0.74	0.73	0.68
Average	**1.89**	**1.55**	**1.02**	**0.65**	**0.63**

List of Figures

periods as the AMS mass-diameter distributions. Valued in all panels are normalized to STP.

Figure S7. Example of the mass-diameter distribution measured by the AMS compared to that derived from the SMPS measurements. The effective particle density ρ_{eff} is determined by the mode diameters. The SMPS mass-diameter distributions were derived by multiplying the SMPS volume-diameter distributions by $\rho_{eff.}$ Data were sampled on March 11, 2008.

Figure S8. (**a**) Time series of the particle volume concentrations obtained by the AMS and the SMPS measurements. (**b**) The ratio of the particle volume concentrations derived from the AMS measurements to the PM_7 light scattering coefficients measured by the nephelometer at 550 nm. The AMS data were averaged to the nephelometer timebase. Gray areas represent the periods that were influenced by the generator exhaust plumes.

Figure S9. Time series of the model residuals e_{ij} for the PMF analysis with *FPEAK* of zero. Terms include factor *j*, time *i*, and error σ.

Figure S10. Pearson's R (black dots) for the correlations between the time series and the mass spectra of any two factors (tagged as x_y) for the PMF solutions for a preset of different number of factors (*p*).

Figure S11. (**a**) The mass spectra of the statistical factors identified by the PMF analysis for four-factor solutions and selected *FPEAK* (f_{peak}) values. (**b**) Time series of mass concentrations for the statistical factors.

Figure S12. The mass spectrum of HOA from the bootstrapping analysis of four-factor PMF solutions. Average (black) with 1-σ error bars (red) are shown.

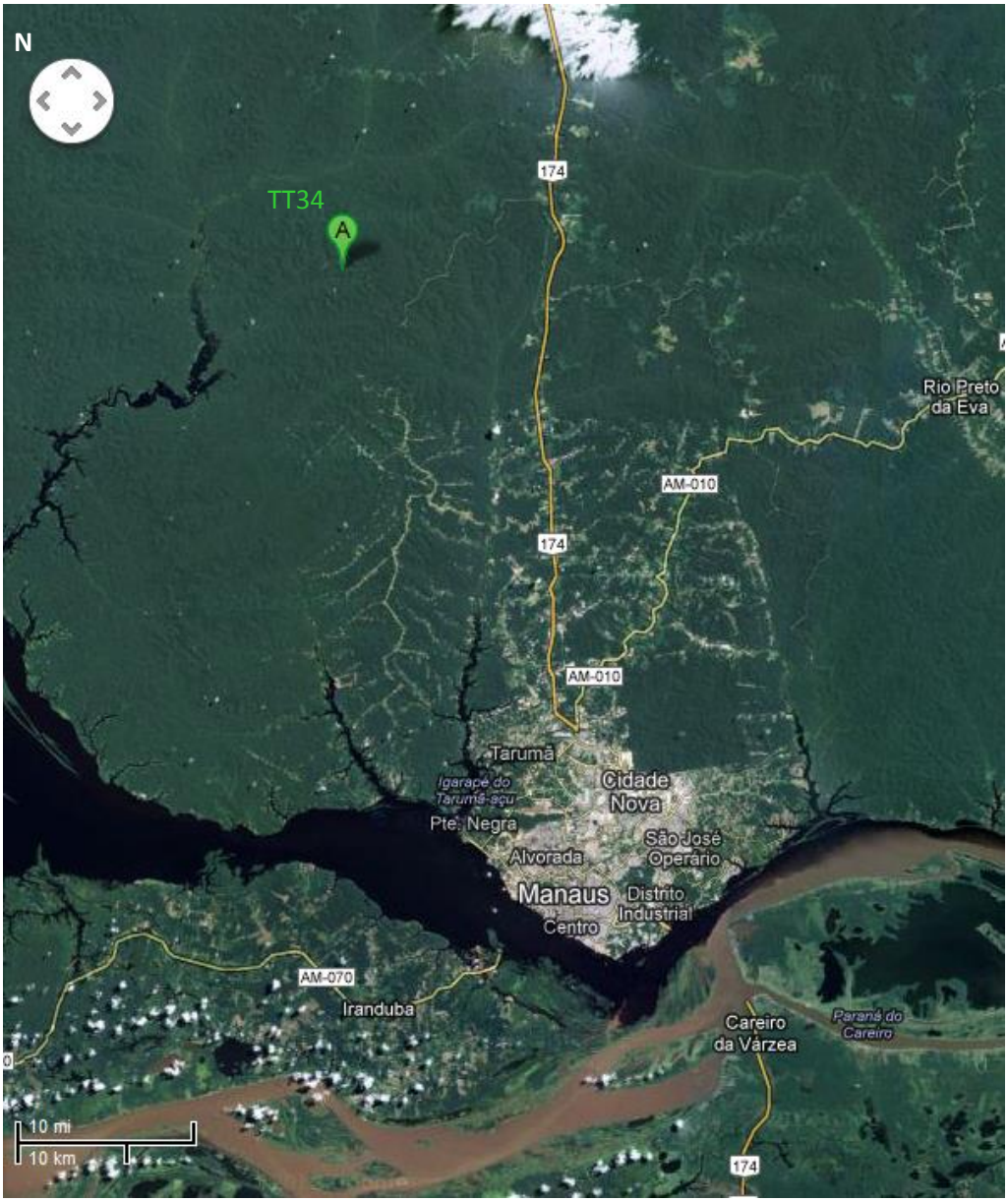
N
TT34
A
174
Rio Preto
da Eva
AM-010
174
AM-010
Tarumã
Igarapé do
Tarumã-açu
Cidade
Nova
Pte. Negra
São José
Operário
Alvorada
Manaus
Distrito
Industrial
Centro
AM-070
Iranduba
Careiro
da Várzea
Paraná do
Careiro
10 mi
10 km
174

Figure S1

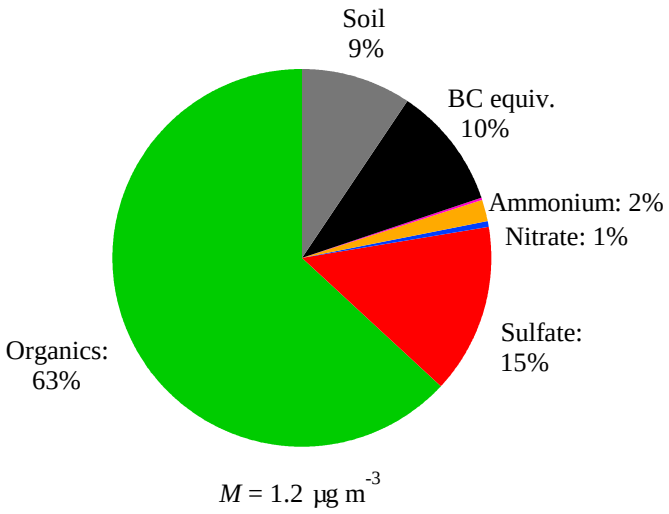
Soil
9%
BC equiv.
10%
Ammonium: 2%
Nitrate: 1%
Sulfate:
15%
Organics:
63%
M = 1.2 µg m-3

Figure S2

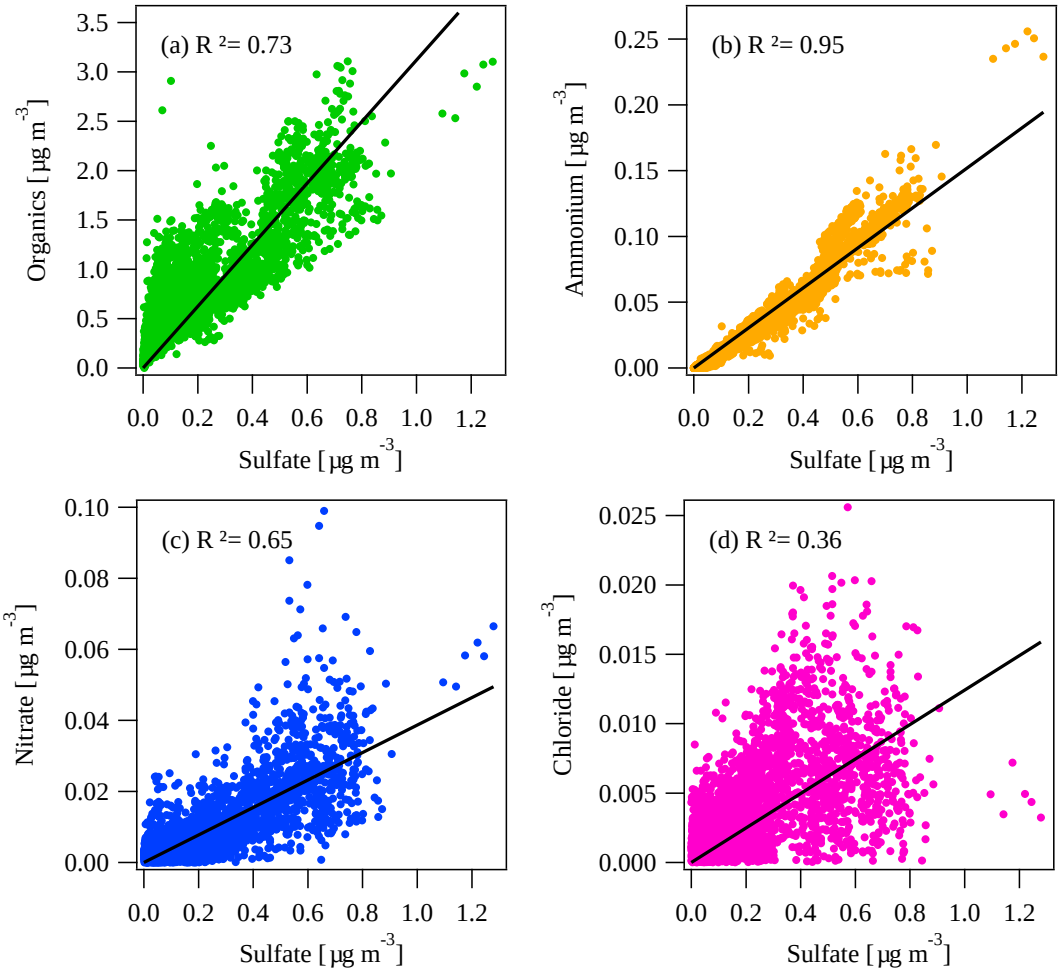
(a) R ²= 0.73
Organics [µg m-3]
Sulfate [µg m-3]
(b) R ²= 0.95
Ammonium [µg m-3]
Sulfate [µg m-3]
(c) R ²= 0.65
Nitrate [µg m-3]
Sulfate [µg m-3]
(d) R ²= 0.36
Chloride [µg m-3]
Sulfate [µg m-3]

Figure S3

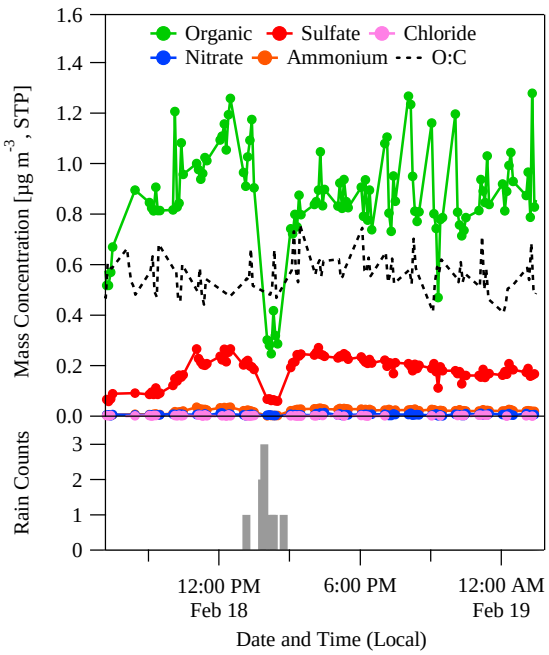
Organic
Sulfate
Chloride
Nitrate
Ammonium
O:C
Mass Concentration [µg m-3, STP]
1.6
1.4
1.2
1.0
0.8
0.6
0.4
0.2
0.0
Rain Counts
3
2
1
0
12:00 PM
Feb 18
6:00 PM
12:00 AM
Feb 19
Date and Time (Local)

Figure S4

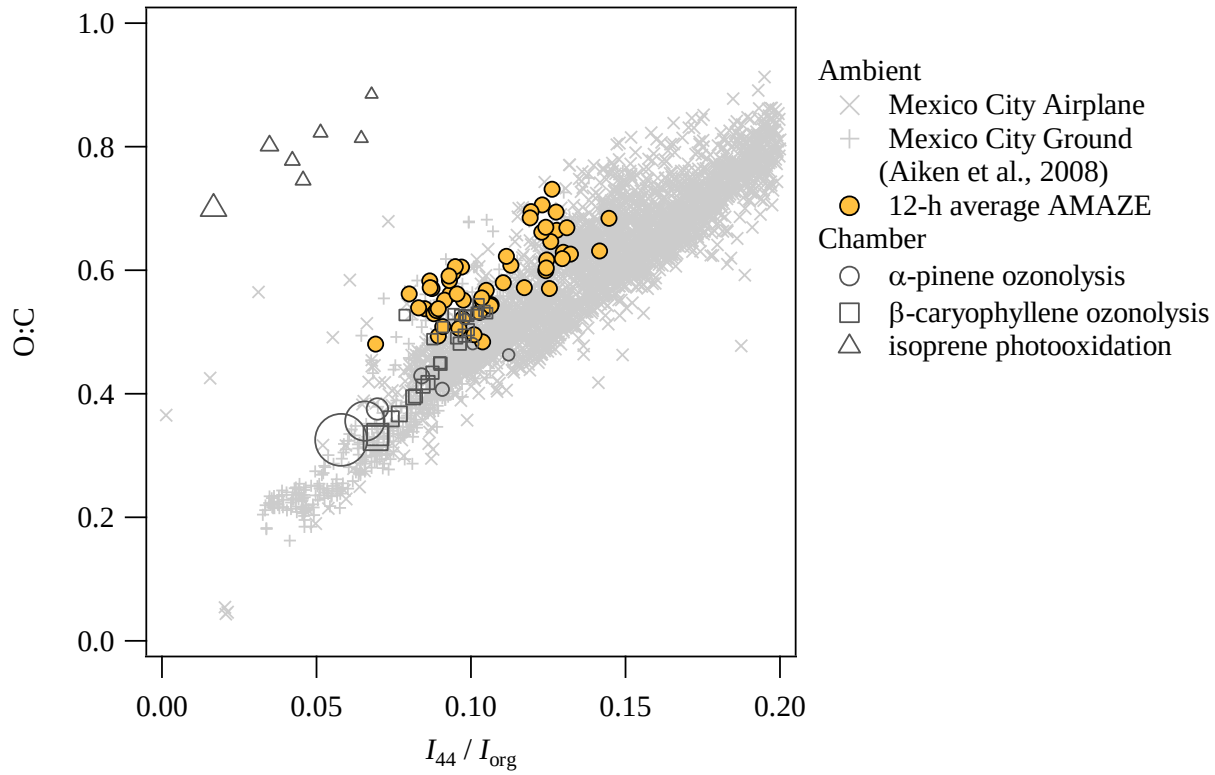
1.0
0.8
0.6
0.4
0.2
0.0
O:C
0.00
0.05
0.10
0.15
0.20
I_{44} / I_{org}
Ambient
Mexico City Airplane
Mexico City Ground
(Aiken et al., 2008)
12-h average AMAZE
Chamber
α-pinene ozonolysis
β-caryophyllene ozonolysis
isoprene photooxidation

Figure S5

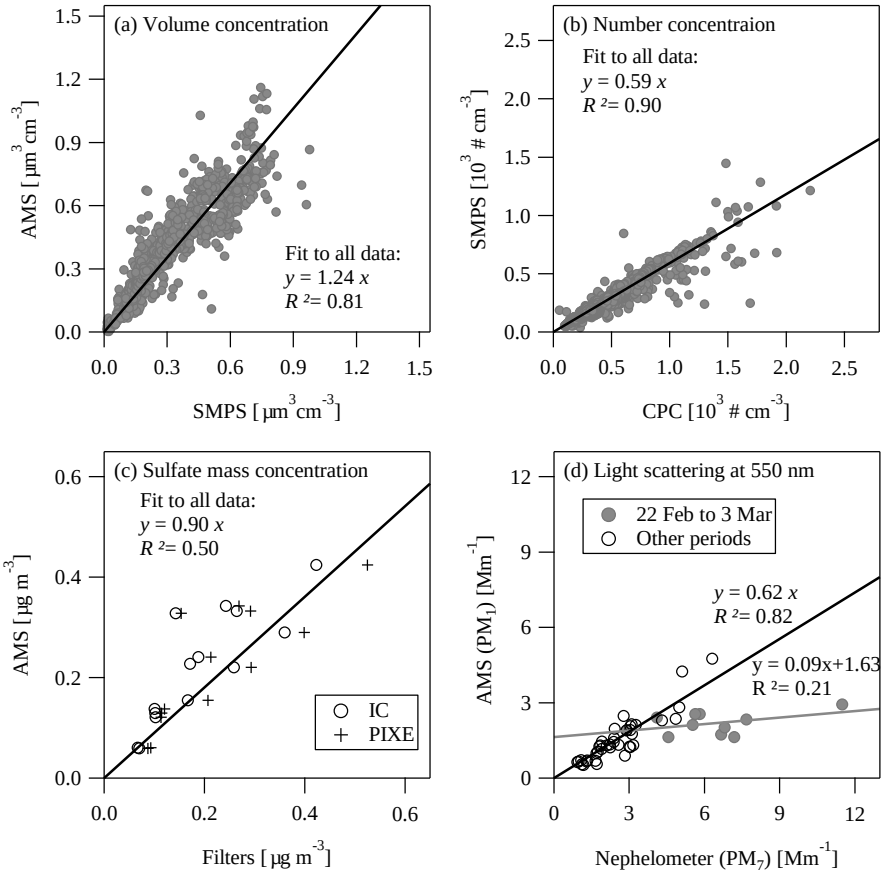
(a) Volume concentration
Fit to all data:
y = 1.24 x
R ²= 0.81
AMS [µm ³ cm ⁻³]
SMPS [µm³ cm⁻³]
(b) Number concentraion
Fit to all data:
y = 0.59 x
R ²= 0.90
SMPS [10³ # cm⁻³]
CPC [10³ # cm⁻³]
(c) Sulfate mass concentration
Fit to all data:
y = 0.90 x
R ²= 0.50
IC
PIXE
AMS [µg m⁻³]
Filters [µg m⁻³]
(d) Light scattering at 550 nm
22 Feb to 3 Mar
Other periods
y = 0.62 x
R ²= 0.82
y = 0.09x+1.63
R ²= 0.21
AMS (PM1) [Mm⁻¹]
Nephelometer (PM7) [Mm⁻¹]

Figure S6

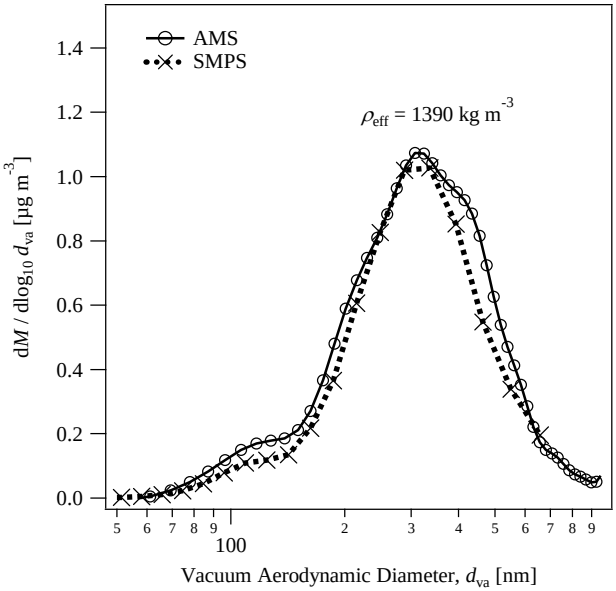
AMS
SMPS
ρ_{eff} = 1390 kg m^{-3}
dM / dlog$_{10}$ d_{va} [µg m^{-3}]
1.4
1.2
1.0
0.8
0.6
0.4
0.2
0.0
5 6 7 8 9
100
2 3 4 5 6 7 8 9
Vacuum Aerodynamic Diameter, d_{va} [nm]

Figure S7

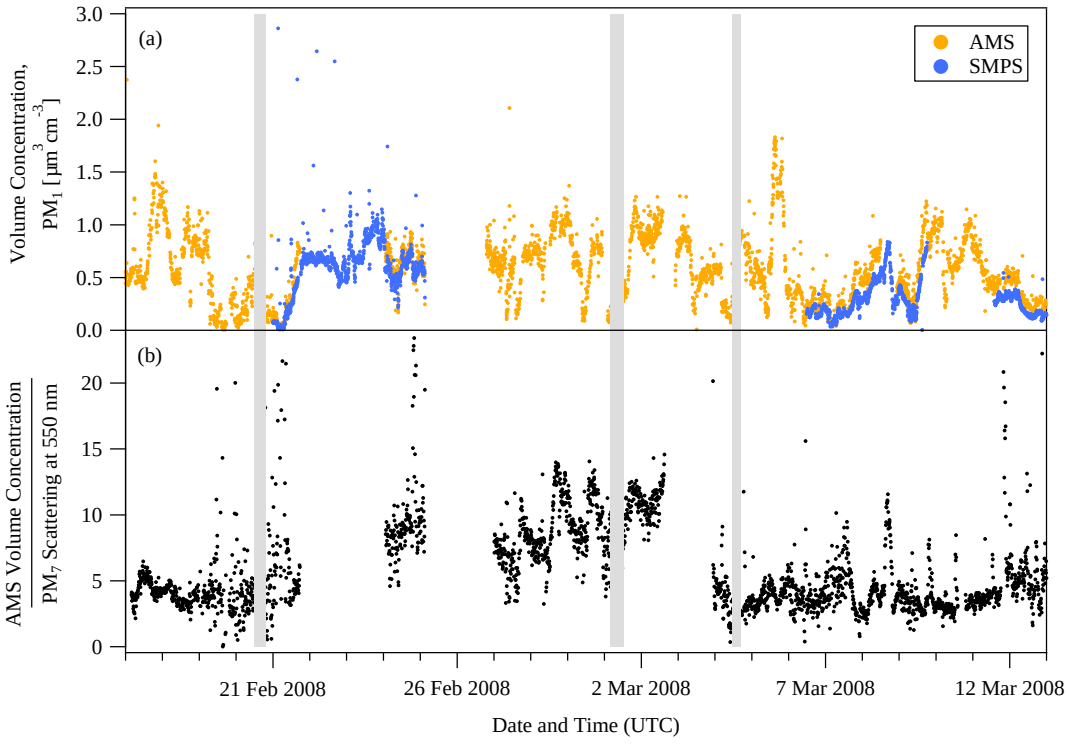
(a)
AMS
SMPS
Volume Concentration, PM1 [μm3 cm-3]
3.0
2.5
2.0
1.5
1.0
0.5
0.0
(b)
AMS Volume Concentration / PM7 Scattering at 550 nm
20
15
10
5
0
21 Feb 2008
26 Feb 2008
2 Mar 2008
7 Mar 2008
12 Mar 2008
Date and Time (UTC)

Figure S8

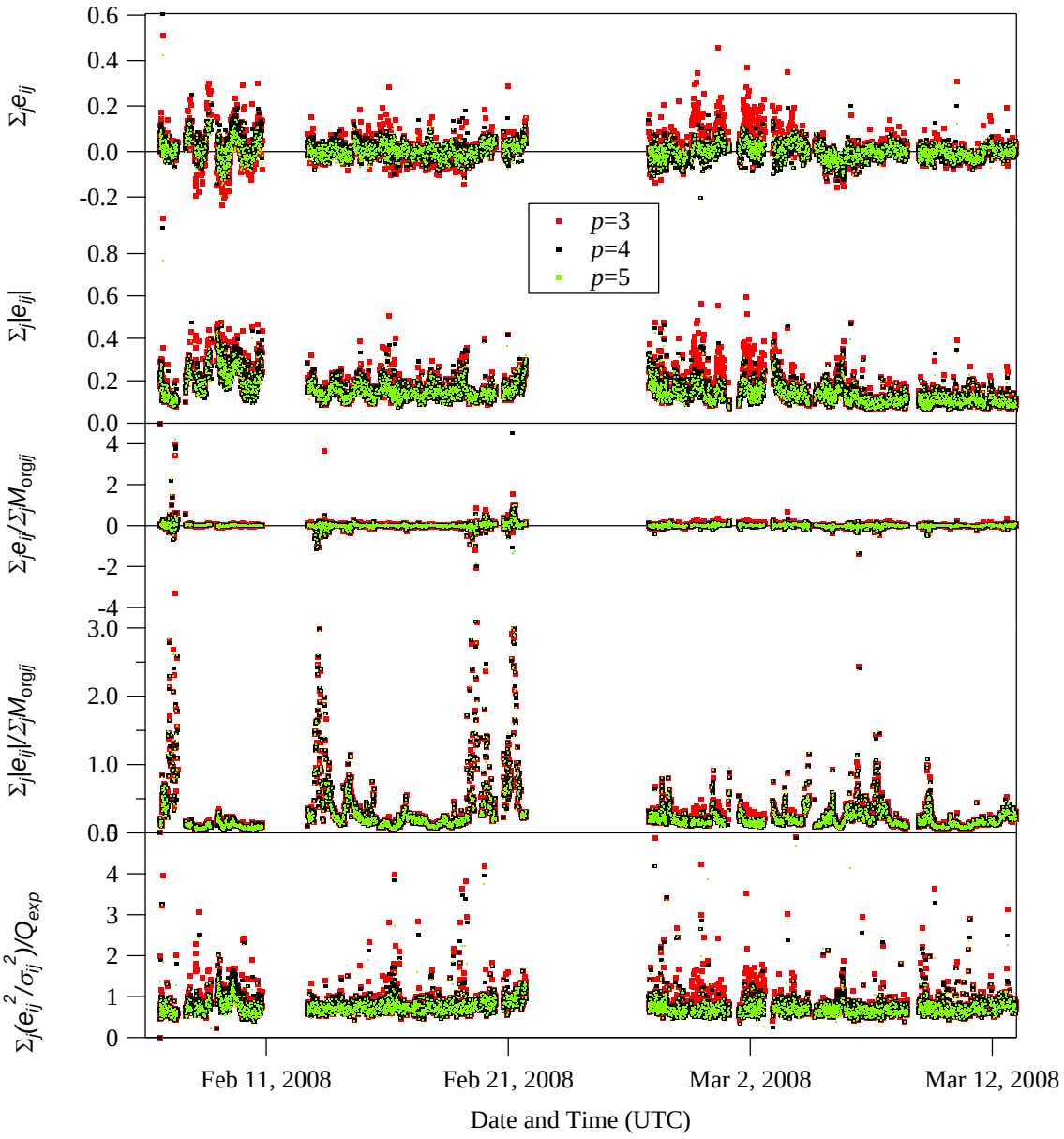
$\Sigma_j e_{ij}$
$\Sigma_j |e_{ij}|$
$\Sigma_j e_{ij} / \Sigma_j M_{orgij}$
$\Sigma_j |e_{ij}| / \Sigma_j M_{orgij}$
$\Sigma_j (e_{ij}^2 / \sigma_{ij}^2) / Q_{exp}$
p=3
p=4
p=5
Feb 11, 2008
Feb 21, 2008
Mar 2, 2008
Mar 12, 2008
Date and Time (UTC)

Figure S9

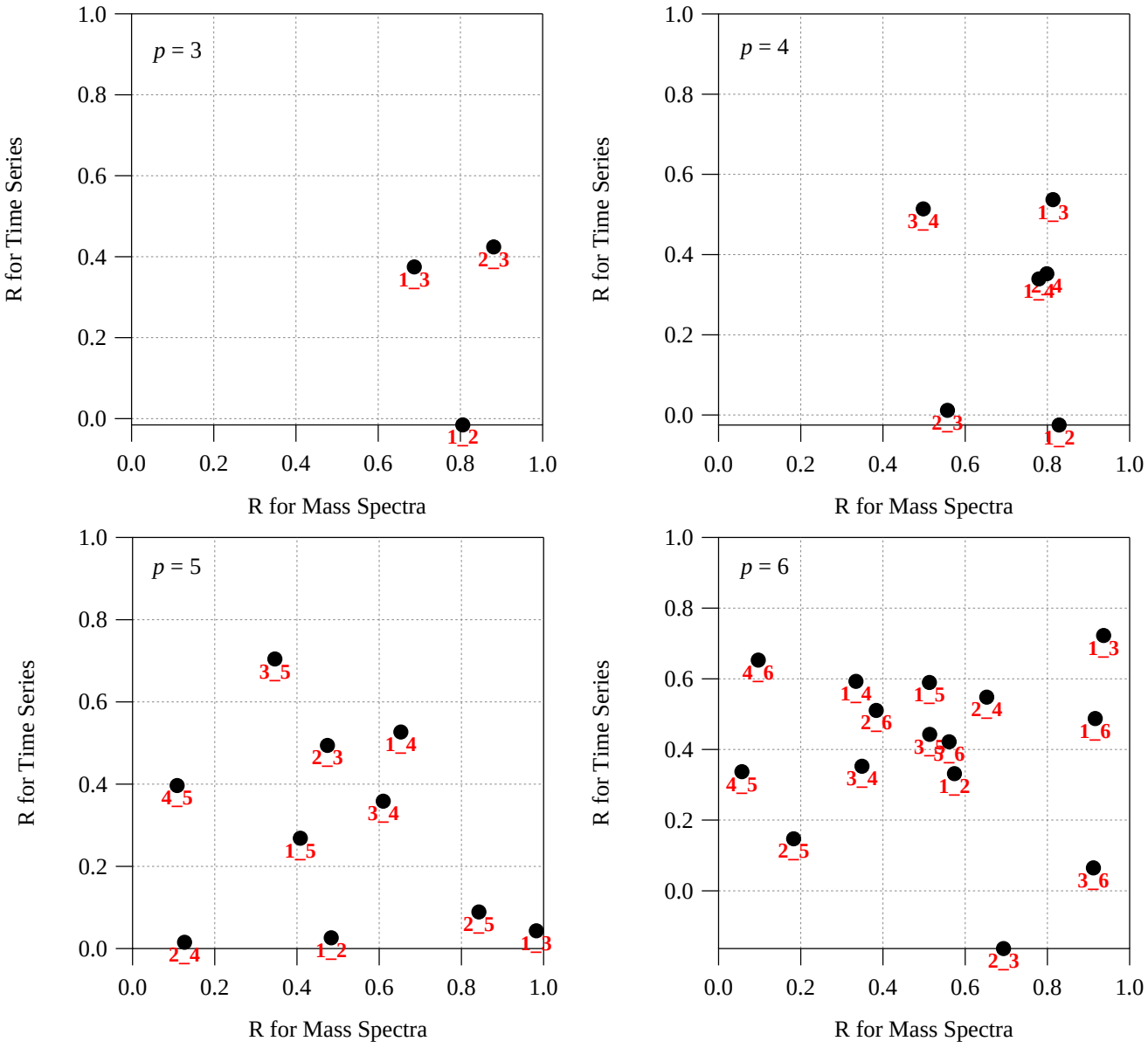
p = 3
1_3
2_3
1_2
p = 4
3_4
1_3
1_4
2_3
1_2
p = 5
3_5
2_3
1_4
4_5
3_4
1_5
2_5
2_4
1_2
1_3
p = 6
4_6
1_4
1_5
2_4
1_3
2_6
3_5
3_6
1_6
4_5
3_4
1_2
2_5
3_6
2_3
R for Time Series
R for Mass Spectra
0.0
0.2
0.4
0.6
0.8
1.0

Figure S10

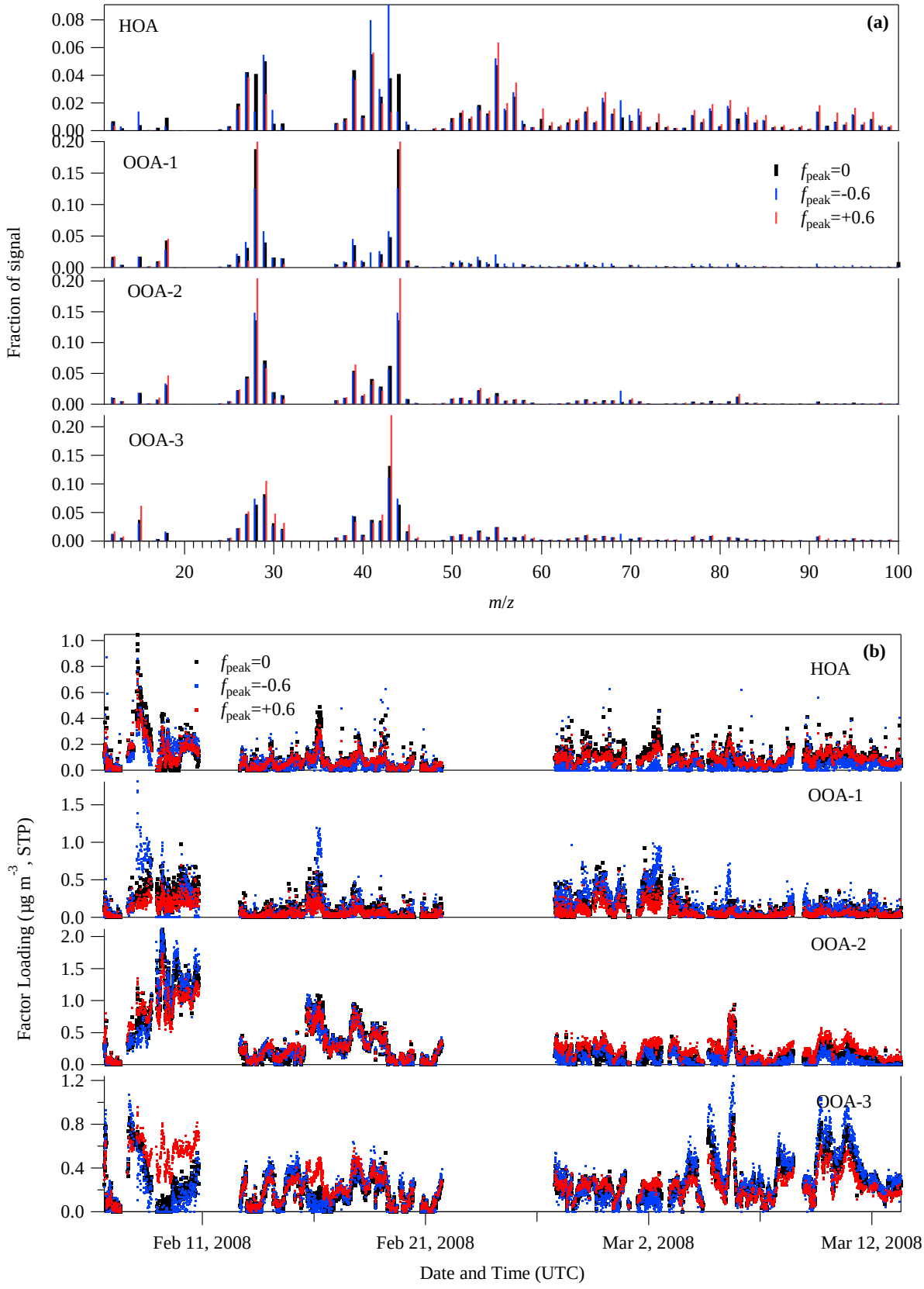
(a)
HOA
OOA-1
OOA-2
OOA-3
f_{peak}=0
f_{peak}=-0.6
f_{peak}=+0.6
Fraction of signal
m/z
(b)
HOA
OOA-1
OOA-2
OOA-3
Factor Loading (μg m^{-3}, STP)
Feb 11, 2008
Feb 21, 2008
Mar 2, 2008
Mar 12, 2008
Date and Time (UTC)

Figure S11

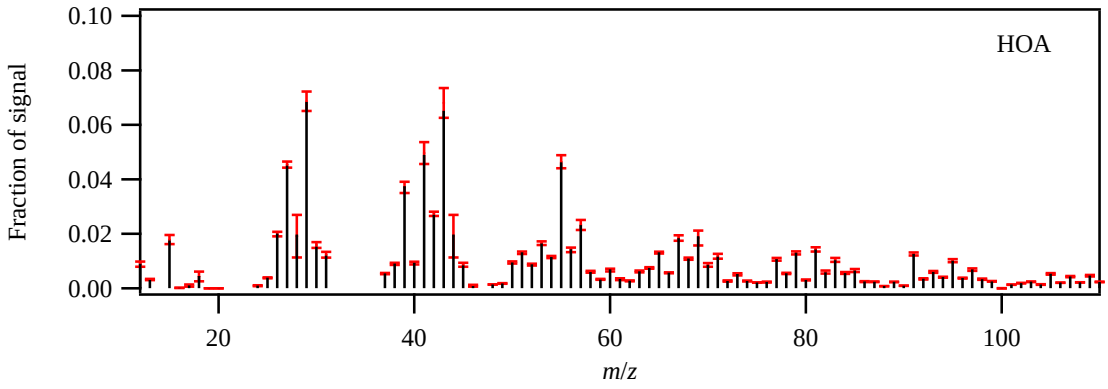
HOA
Fraction of signal
0.10
0.08
0.06
0.04
0.02
0.00
20
40
60
80
100
m/z

Figure S12